water

MDPI

Article

NaOH-Activated Natural Glauconite for Low-Cost Adsorption of Congo Red Dye

Ahmed Hamd [1], Doaa Salah [2,3], Huda Fadol Alyafei [4], Nofal K. Soliman [1], Ahmed A. M. El-Reedy [1], Ali M. Elzanaty [2], Sameerah I. Al-Saeedi [5], Azza Al-Ghamdi [6,7], Mohamed Shaban [8,*], Refat El-Sayed [9,10] and Sayed A. Ahmed [2,11]

[1] Basic Science Department, Faculty of Oral and Dental Medicine, Nahda University, Beni Suef 62764, Egypt
[2] Department of Chemistry, Faculty of Science, Beni-Suef University, Beni Suef 62511, Egypt
[3] Nanophotonics and Applications (NPA) Lab, Physics Department, Faculty of Science, Beni-Suef University, Beni Suef 62514, Egypt
[4] Math, Statistics and Physics Department, College of Art and Science, Qatar University, Doha P.O. Box 2713, Qatar
[5] Department of Chemistry, Collage of Science, Princess Nourah bint Abdulrahman University, P.O. Box 84428, Riyadh 11671, Saudi Arabia
[6] Department of Chemistry, College of Science, Imam Abdulrahman Bin Faisal University, P.O. Box 1982, Dammam 31441, Saudi Arabia
[7] Basic & Applied Scientific Research Center (BASRC), Renewable and Sustainable Energy Unit, Imam Abdulrahman Bin Faisal University, P.O. Box 1982, Dammam 31441, Saudi Arabia
[8] Department of Physics, Faculty of Science, Islamic University of Madinah, P.O. Box 170, Madinah 42351, Saudi Arabia
[9] Department of Chemistry, University College in Al-Jamoum, Umm Al-Qura University, Makkah 21955, Saudi Arabia
[10] Chemistry Department, Faculty of Science, Benha University, Benha 13511, Egypt
[11] Basic Science Department, Faculty of Engineering, Nahda University, Beni Suef 62764, Egypt
* Correspondence: mssfadel@aucegypt.edu

Abstract: To explore the adsorption of Congo red (CR) dye from textile effluent, natural clay glauconite was employed as a sustainable and inexpensive adsorbent. The effects of varying concentrations of sodium hydroxide (NaOH) on glauconite alteration were examined. Furthermore, this research focuses on the optimal NaOH concentration that improves removal efficiency and adsorption capacity. Thus, four NaOH solutions of concentrations ranging from 1 M to 4 M were used to activate glauconite raw (GL), indicated as GLACT1M, GLACT2M, GLACT3M, and GLACT4M. These samples were characterized using different analysis tools. The effects of starting concentration, adsorption time, adsorbent dosage, pH, temperature, and reusability on removal efficacy were all investigated. The data show that the CR removal efficiency increases with modification up to a 2 M NaOH activation, beyond which it begins to decrease. At 25 °C and pH 7, the CR removal efficiencies were ~77%, 72%, 80%, 34.5%, and 30.5% by GL, GLACT1M, GLACT2M, GLACT3M, and GLACT4M, respectively. Batch experiments were performed to explore both the kinetics and isotherms of CR adsorption to determine the impact of different experimental conditions accurately. Moreover, isotherm interpretations demonstrated that the Freundlich isotherm closely matches the experimental results. The pseudo-second-order model clearly explains the obtained results (R^2 = 0.998) from 5 to 25 ppm for GL, GLACT1M, GLACT2M, and GLACT3M, but GLACT4 is expressed by the Elovich model from 20 to 25 ppm. The reusability investigation revealed that the reusability of adsorbents could be achieved efficiently. The findings suggest that glauconite and its NaOH-activated forms can be employed as natural and affordable adsorbents for removing CR from textile effluent.

Keywords: natural glauconite; NaOH; adsorption; Congo Red Dye; kinetics; isotherms

check for updates

Citation: Hamd, A.; Salah, D.; Alyafei, H.F.; Soliman, N.K.; El-Reedy, A.A.M.; Elzanaty, A.M.; Al-Saeedi, S.I.; Al-Ghamdi, A.; Shaban, M.; El-Sayed, R.; et al. NaOH-Activated Natural Glauconite for Low-Cost Adsorption of Congo Red Dye. *Water* **2023**, *15*, 3753. https://doi.org/10.3390/w15213753

Academic Editors: Tian Li, Shuili Yu and Junxia Liu

Received: 5 September 2023
Revised: 19 October 2023
Accepted: 25 October 2023
Published: 27 October 2023

Copyright: © 2023 by the authors. Licensee MDPI, Basel, Switzerland. This article is an open access article distributed under the terms and conditions of the Creative Commons Attribution (CC BY) license (https://creativecommons.org/licenses/by/4.0/).

1. Introduction

Water scarcity increases day by day due to daily effluents caused by chemical contaminants [1–3]. These contaminants vary from industrial and radioactive wastes to pesticides, mining activities, and chemical fertilizers [3–5]. Dyes represent a great sector of the daily pollutants that contaminate water resources as they are included in different advanced industrial fields like textile, paper, leather tanning, food processing, plastics, cosmetics, rubber, printing, and dye production [6,7]. These systems can be physical, chemical, biological, or mixed systems [3,8–12]. One of the most considered systems is adsorption due to its efficiency, environmental and economic sustainability, and realistic viability in dye removal [13,14]. This system depends mainly on selectively removing dissolved components from aqueous solutions by adhering these dissolved parts onto the surface or within the porous structure of solid objects (adsorbents) [15–19].

Various adsorbing systems have been tested to remove these dyes from wastewater effluent. Due to their availability and abundance, these systems currently utilize a range of naturally occurring ores [20–22]. These clay minerals are classified as a type of layered silicate minerals [5,23–25]. Known and scientifically familiar adsorbing systems include bentonite, expanded vermiculite, montmorillonite, bio-clay composite, and natural illicit clay minerals [26,27]. Furthermore, it has been well established that clay surfaces can be altered to boost their adsorption potential [22,25,27–32]. In comparison, the negative overall charge of silicate clay minerals is balanced with the positive charge of cationic dyes.

The heterogeneous phyllosilicate mineral known as glauconite (GL), which has a bluish-green to greenish-black color and a monoclinic crystal structure with the group space C2/m deposit, was chosen to be the subject of this study's investigation [33]. Its general chemical expression is (K, Na) (Fe, Al, Mg)$_2$(Si, Al)$_4$O$_{10}$(OH)$_2$. Glauconite, green clay, possesses a specific gravity between 2.4 and 2.95, with a molecular weight of 426.93 g. The abundance of GL is usually in the seafloor regions, mainly within the phosphate rocks. The three basic processes that result in the development of GL are the direct precipitation of saltwater, the change of illitic and biotitic clay particles by seawater, and the transformation of pellets made of animal excrement. In the presence of alumina and silica, as well as moderately strong iron and potassium oxides, one di-octahedral layer is wedged between two silicon tetrahedral layers in this clay's structure [34]. GL is a well-known adsorbent that has been investigated in wastewater treatment to remove various metal ions or dyes [25]. According to Sobeih et al. [35], glauconite is a three-layer organic sheet of aluminum silicate that is primarily found in marine sediments. Between two flat siliconate layers with OH groups, it has layers of water molecules and alkaline earth metals, most notably potassium, alternated with multivalent iron, aluminum, and magnesium ions [35]. Where NaCl- and NaOH-treated glauconite-carrying sands were applied for removing uranium and thorium [36], dyes [37], metals and ammonium [38], and phosphate [39], it is expected that glauconite possesses a metal-adsorbing capacity. Glauconite was employed by Ali et al. [36] to extract uranium and thorium from aqueous solutions. Petrushka et al. investigated the kinetics of the anionic red 8C dye's adsorption on glauconite [37]. Natural glauconite has been tested by Hao and co-workers in the removal of heavy metals (Zn, Pb, Cd) and ammonia [38]. Due to the poor results obtained by the last study, glauconite has been modified to improve its characteristics [35,39]. Younes et al. hypothesized that modified glauconite with thermal and acetic acid would be effective for removing reactive yellow 160 dye from textile effluent [39]. A high adsorption capacity is also obtained by modifying glauconite with chitosan nanocomposites to remove fluoride ions from liquids. Furthermore, the chitosan-modified glauconite was effectively used to remove fluoride ions from liquids with an adequate adsorption capacity [35]. However, to shorten the processing time and increase the effectiveness of glauconite as an adsorbent, a low-cost activation procedure for glauconite is necessary since the efficiency that has been achieved in previous studies is low, and the processing time is still lengthy.

It is still highly favored to synthesize adsorbents with low production costs, strong recyclability, and high adsorption capacities. Consequently, how the concentration of the

NaOH solution affects the adsorption behavior of the NaOH-activated glauconite clay in the removal of CR has not yet been documented. The newly developed nano adsorbent is also relatively inexpensive and highly effective, and it processes more quickly than earlier adsorbents utilized for CR removal. Additionally, it can remove CR from water more quickly and efficiently than other methods. When there is a critical need for time, such as during an emergency response or when handling a sizable amount of contaminated water, this can be useful. The current study is considered the first on glauconite extracted from deep mines in the Abu-Tartor region in Egypt. This area is believed to have a more active glauconite type due to the presence of large deposits of phosphate rock around the clay. The study targets the characteristics and adsorption impact of natural glauconite and its NaOH-activated derivatives on polluted wastewater with CR dye of varied concentrations. The influences of starting dye concentration, adsorption period, adsorbent dosage, pH, temperature, and reusability are investigated and optimized to produce an efficient nano adsorbent for CR dye removal. The kinetics and thermodynamics of the adsorption are investigated.

2. Materials and Methods

2.1. Materials

Glauconite was mined and supported by the aid of the Phosphat-Misr company for mining. Sodium hydroxide pellets (99.99%), 36% hydrochloric acid, and CR dye (99.99%) were bought from Sigma-Aldrich (Darmstadt, Germany). All these chemicals were used without further purification. Distilled water was used as the dissolving medium in all reactions.

2.2. Glauconite Activation

Four concentrations from the NaOH solution were prepared (1 M, 2 M, 3 M, and 4 M) and used as an activating medium for the glauconite with a 10:1 ratio of NaOH/glauconite [40]. All samples were then subjected to a heating process at 373 K for 4 h with continuous stirring at 500 rpm for 1 h. The resulting activated glauconite was filtered and washed with distilled water (DW) numerous times to remove excess NaOH and neutralize the pH before being crushed and sieved into 315 µm.

2.3. Instrumentations/Characterizations

To identify the crystallographic and structural properties of the produced samples, the X-ray diffraction (XRD, Philips X'Pert Pro MRD, Almelo, The Netherlands) examination was used with CuK_{α} radiation = 1.5418 Å, operated at 20 mA and 40 kV in the 2θ range of 5–70 at a scanning speed of 5°/min [25]. A scanning electron microscope (SEM, JEOL JSM-5400 LV, Tokyo, Japan) was employed to determine the morphologies of the samples [25]. To determine the functional groups, Fourier-transform infrared (FT-IR, Bruker Vertex 70 FTIR-FT, Billerica, MA, USA) spectra of the manufactured samples were investigated using the dry KBr pellet method.

2.4. Preparation of Adsorbate

For the current study, anionic CR dye ($C_{32}H_{22}N_6Na_2O_6S_2$) was selected to be the adsorbate of choice. A total of 1.0 g of CR was hydrated in 1 L of DW as a solvent to obtain a 1000 mg/L stock solution. A dilution process was applied using distilled water for the preparation of the required CR solutions for batch experiments. The pH of the prepared solutions was controlled at values of 2, 4, 6, 8, and 12 using solutions of either 0.1 M HCl or NaOH [25].

2.5. Adsorption Studies

A total of 420 min in batch mode experiments were applied for all CR dye adsorption investigations under various conditions. Initial concentrations of 5 to 25 mg/L, contact times ranging from 0 to 420 min, adsorbent doses of 0.02 to 0.1 g per 20 mL of CR solutions,

a pH range of 2 to 12, and temperature gradients ranging from 25 to 90 °C were all employed. Table S1 (Supplementary Materials) shows four adsorption experiment series performed on GL, GLACT1M, GLACT2M, GLACT3M, and GLACT4M adsorbents under various adsorption conditions. The absorption peaks were measured using the UV-Vis spectrophotometer (Perkin Emer, Lambada 950, Waltham, MA, USA) and used to detect variations in the concentrations of tested dyes.

Adsorbent reusability studies were carried out seven times, each time utilizing 0.02 g of the targeted adsorbent and 20 mL of 5 mg/L CR for 120 min at 25 °C. After each run, the adsorbent was removed from the solution and washed with DW before reusability.

Using Equations (1)–(3), the amount of dye adsorption by the prepared samples at equilibrium (q_e(mg/g)) and at time t (q_t), as well as the CR dye removal%, were computed [31,35]:

$$q_e = (C_o - C_e)\frac{V}{m} \quad (1)$$

$$q_t = (C_o - C_t)\frac{V}{m} \quad (2)$$

$$\text{CR dye removal \%} = \frac{(C_o - C_t)}{C_o} \times 100 \quad (3)$$

C_o, C_t, and C_e are the CR concentrations at the starting, at time t, and at equilibration, correspondingly. "m" represents the tested mass of the adsorbent, whereas V represents the volume of dye.

2.6. Adsorption Isotherms

To understand how dissolved ions settle on solid adsorbents, adsorption data must be fitted to isotherm models [41]. Three isotherms' models, Langmuir, Freundlich, and Temkin, were used to better understand the CR dye adsorption behavior on glauconite derivatives (GL, GLACT1M, GLACT2M, GLACT3M, and GLACT4M) [42].

The Langmuir adsorption isotherm is presented by Equation (4):

$$\frac{C_e}{q_e} = \frac{1}{K_L Q_o} + \frac{C_e}{Q_o} \quad (4)$$

where q_e is the amount of CR adsorbed/unit mass, Q_o is the maximum quantity of dye that an adsorbent can remove in mg/g, and K_L is the Langmuir equilibrium constant.

The Freundlich adsorption isotherm is presented by Equation (5):

$$logq_e = logK_F + \frac{1}{n} logC_e \quad (5)$$

where K_F is the Freundlich constant, and the adsorption density is denoted by n.

The Temkin adsorption isotherm is presented by Equation (6):

$$q_e = Bln(K_T) + Bln(C_e) \quad (6)$$

where K_T is the Temkin constant and the heat of the adsorption-related constant is B = RT/b. T is the absolute temperature, and R is the universal gas constant. The dimensionless factor, R_L, in Equation (7) describes the equilibrium data and can be used to estimate the favorableness of the Langmuir isotherms [43].

$$R_L = \frac{1}{(1 + K_L C_{max})} \quad (7)$$

where C_{max} indicates the maximum starting CR concentration.

2.7. Adsorption Mechanisms and Kinetics

The adsorption mechanisms and kinetics of CR over GL, GLACT1M, GLACT2M, GLACT3M, and GLACT4M nanoadsorbents were assessed using a variety of adsorption mechanisms and kinetic models. Pseudo-first-order and second-order kinetic, Elovich kinetic, and intra-particle diffusion models were employed according to Equations (8)–(11) [24,25].

The Pseudo-first-order kinetic model is given by Equation (8):

$$Ln\ (q_e - q_t)\ =\ ln\ q_e - k_1 \cdot t \tag{8}$$

The Pseudo-second-order kinetic model is given by Equation (9):

$$\frac{t}{q_t}\ =\ \frac{1}{k_2 q_e^2} + \frac{t}{q_e} \tag{9}$$

The Elovich kinetic model is given by Equation (10):

$$q_t\ =\ \frac{1}{\beta} lnln\ \alpha\beta + \frac{1}{\beta} lnln\ t \tag{10}$$

The intra-particle diffusion model can be represented by Equation (11):

$$q_t\ =\ k_3 t^{\frac{1}{2}} + I \tag{11}$$

where k_1, k_2, and k_3 are the rate constants for the pseudo-first-order, pseudo-second-order, and intra-particle propagation. α indicates the starting reaction rate (mg/min), β signifies the surface coverage extent (g/mg), and I is a measure of the thickness of the boundary layer.

2.8. Statistical Analyses

The adsorption records were calculated as an average of triplicate measurements. Using statistical tools in OriginPro 2016 and Microsoft Excel 2010, the regression coefficients (R^2) of the Elovich kinetic, intra-particle diffusion, pseudo-first-order, and pseudo-second-order models were found.

3. Results and Discussion

3.1. Adsorbent Characterization

3.1.1. Morphological Study

Figure 1a–c illustrate glauconite particles in the form of granules with an expanded structure and a layered morphology. The presence of agglomerates exhibiting delicate, flaky shapes in natural samples indicates the presence of smectites. The alkaline treatment had minimal impact on the specific surface area of the mineral. This is likely due to the combined effects of two factors: the dissolution of swelling layers along tetrahedral planes and the amorphization of the surface resulting from the formation of insoluble sodium silicates [40].

Figure 1d–o show SEM images of the activated samples with 1 M, 2 M, 3 M, and 4 M NaOH solutions. Upon activation of glauconite nanoparticles with NaOH solutions of varying concentrations, a self-assembly process occurs, resulting in more uniform surfaces with apparent nanoporous characteristics. As the NaOH increased from 1 M to 2 M, Figure 1d–i, the density of the nanopores increased. Figure 1j–o illustrate how the particle size decreases and the nanoporous features weaken and ultimately disappear when the NaOH concentration rises from 3 M to 4 M, enabling GLACT4M to form compacted GL microstones. In the cases of GLACT3M and GLACT4M, the glauconite particles exhibit greater homogeneity and compactness. These morphological observations suggest that the GLACT2M sample may be the most suitable activated sample for efficient dye adsorption on its surface, owing to its nanoporous nature.

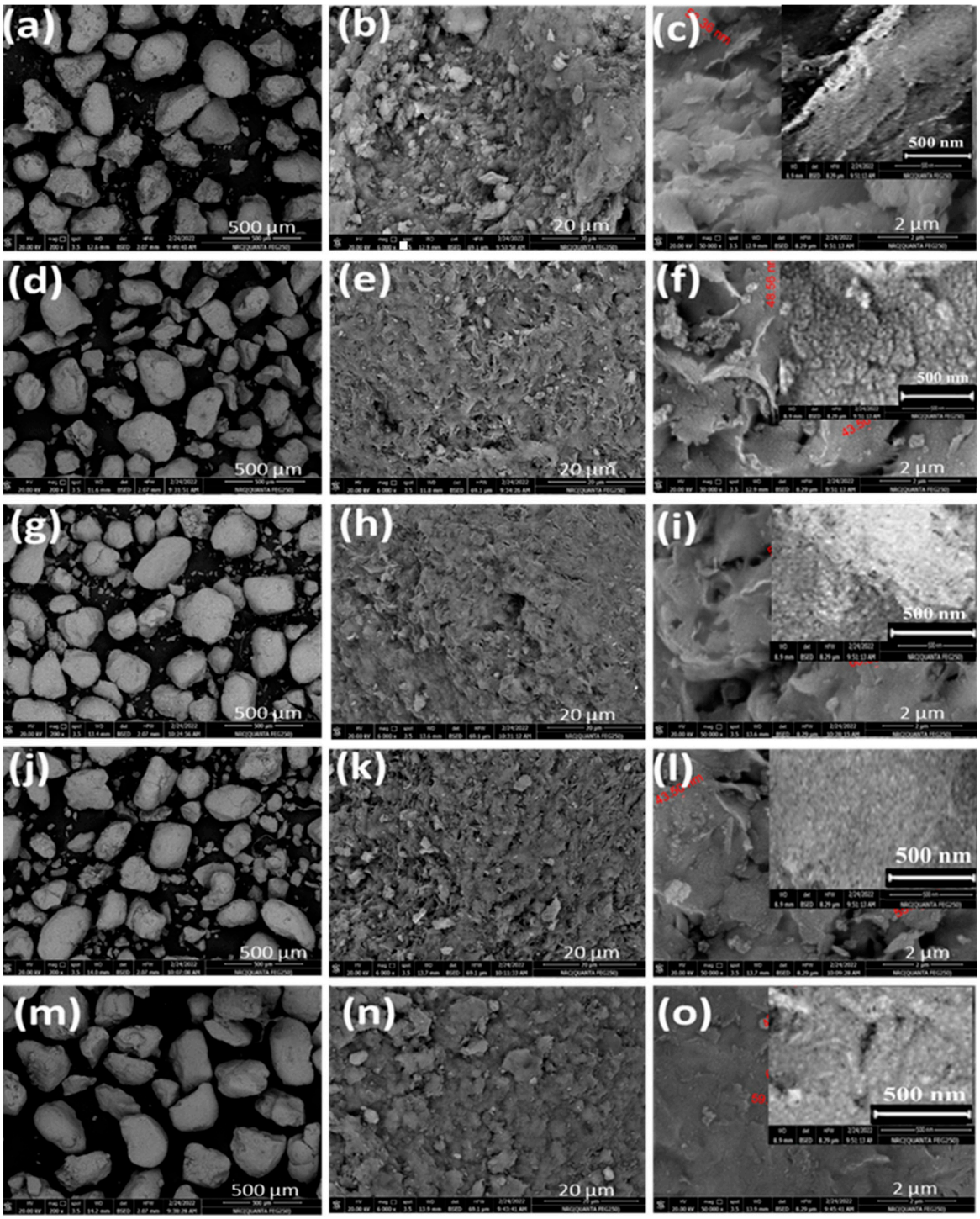


Figure 1. SEM images of (**a**–**c**) raw GL and (**d**–**o**) activated GL samples with NaOH; (**d**–**f**) GLACT1M, (**g**–**i**) GLACT2M, (**j**–**l**) GLACT3M, and (**m**–**o**) GLACT4M.

3.1.2. Functional Groups and Crystallographic Structures

The functional groups of glauconite and its activated forms are explored using FT-IR spectroscopy ranging from 4000 to 400 cm^{-1}. The FT-IR spectra in Figure 2a exhibited broad modes at 3400–3700 cm^{-1} generated by OH-stretching vibrations (OHv; 3700–3500 cm^{-1}) and OH-bending vibrations (OHδ) [44]. The features in FTIR spectra show $Fe^{3+}OHFe^{3+}$ (at about 3507 cm^{-1}) and $Fe^{3+}OHMg$ (at about 3640 cm^{-1}) bands in OH-stretching zones [44]. The spectra included vibrational modes at 802 and 1023 cm^{-1}, assigned to Fe–OH bend-

ing and Si(Al)–O–Si asymmetric stretching, correspondingly. Meanwhile, the band that appeared at 1640 cm^{-1} is related to the H–O–H bending mode (v_2 mode) [45]. The bending vibrational mode of the Si–O bond appears at 678 cm^{-1}. The bending vibrational modes related to Si–O–Mg, Si–O–Si, and Si–O–Fe^3 appear at 445, 447, and 496 cm^{-1} correspondingly [39]. So, activation with NaOH of different concentrations did not change the structure of raw material; it just enhanced its physical properties within dye adsorption. Table 1 summarizes the main vibrational bands of the prepared samples and their assignments [35,39,46–49]. Figure S1 (Supplementary Materials) reveals the interaction between the phyllosilicate clay mineral (glauconite) and different function groups found in Congo red dye. These interactions are summarized in hydrogen bonds and electrostatic attractions between different active sites and free function groups on both clay and dye, respectively.

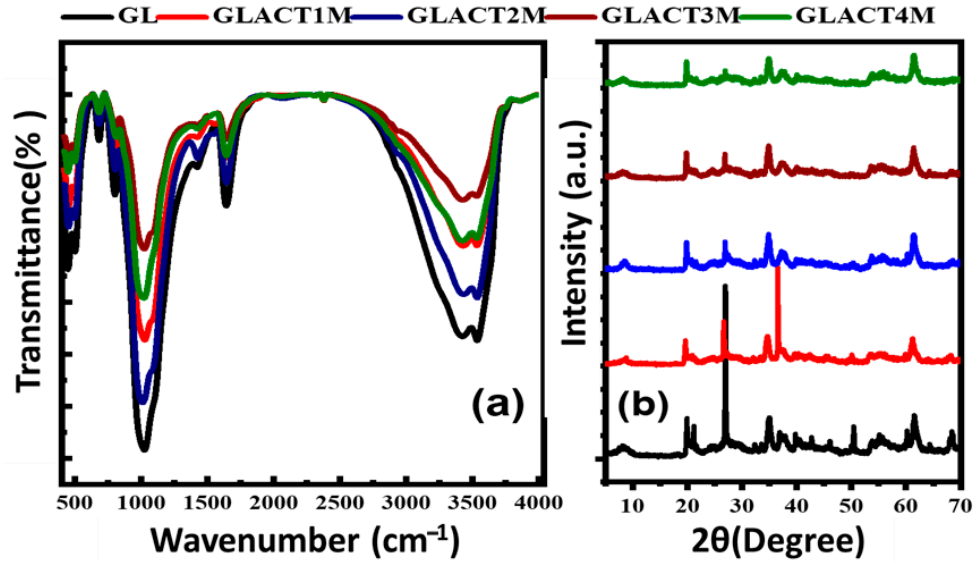


Figure 2. (**a**) FT-IR and (**b**) XRD patterns of GL and the activated GL samples.

Table 1. The vibrational modes and their functional groups for GL, GLACT1M, GLACT2M, GLACT3M, and GLACT4M.

Peak Position (cm^{-1})					Functional Group	Ref.
GL	GLACT1M	GLACT2M	GLACT3M	GLACT4M		
445–498	450–488	450–496	450–496	445–496	Si–O–Fe & Si–O–Mg	[35,39,46–49]
680	681	681	681	680	OH or Si–O bond	
800	794	803	802	809	Al Fe–OH	
1023	1025	1009	1022	1018	Si–O–Si	
1421	1421–1555	1424	1423–1514	1422	C–H	
1640	1640	1641	1640	1641	H–O–H & C = O	
3422–3533	3420–3532	3430–3533	3425–3530	3424–3531	O–H and/or N–H	

X-ray diffraction (XRD) is used to examine the materials' crystallographic structures. Glauconite is a greenish-colored, very crumbly iron potassium phyllosilicate (mica group) mineral. Glauconite's principal chemical composition does not contain sodium oxide [50]. Figure 2b illustrates XRD charts for GL, GLACT1M, GLACT2M, GLACT3M, and GLACT4M. The diffraction patterns of the produced samples are quite close to those of Gl [50]. Glauconite matches the majority of known phyllosilicates, according to Selim et al. [47] in their investigation of Egyptian phyllosilicates. The most obvious peaks at 2θ of 21.3° and 27.8° demonstrate the presence of GL in the samples. In certain instances, the appearance of strong peaks denotes the presence of other clays, like kaolinite and quartz, within the structure of the phyllosilicate clay mineral. However, the sharp peak shifts to a

lower 2θ-angle with a considerable drop in intensity, indicating the role of NaOH in GL activation. The strength of this peak diminished as the concentration of the NaOH solution rose. After the activation process, the original structure of the GL may be seen to be slightly retained. The major effect of the NaOH treatment appears to be a small decrease in the crystallinity, most notably the (003) peak in Figure 2b. The Scherer equation, $D = 0.9\lambda / (\beta \cos\theta)$, was used to calculate the typical crystallite size. The λ, β, and θ are the X-ray wavelength, full width at half maximum, and diffraction angle, correspondingly. The value of D was determined to be ~16 nm for Gl. Due to the polycrystalline structure of GL, the detected nanoparticle in SEM images has at least three crystallites. The minimum dislocation density was estimated from the reciprocal of D^2 to be 3.9×10^{-3} dislocation/nm^2.

3.2. Adsorption of Congo Red

3.2.1. Effects of Starting Dye Concentration

Figures 3 and S2 (Supplementary Materials) depict the variation of the dye removal% and amount of adsorbed CR dye versus time by GL, GLACT1M, GLACT2M, GLACT3M, and GLACT4M at different initial dye concentrations. These graphs show that the initial stages of the adsorption process were characterized by high adsorption capacities and removal percentages, which then gradually declined until equilibrium was reached. There may be a significant number of exposed active adsorption sites on the surface of the adsorbent, which could explain why the removal rate was so high at the beginning of the operation. When the contact time is increased to 360 min, the exposed sites are completely occupied by the adsorbed CR molecules, and CR molecules compete for limited binding sites, so the removal rate decreases until it reaches the equilibrium state [25,49].

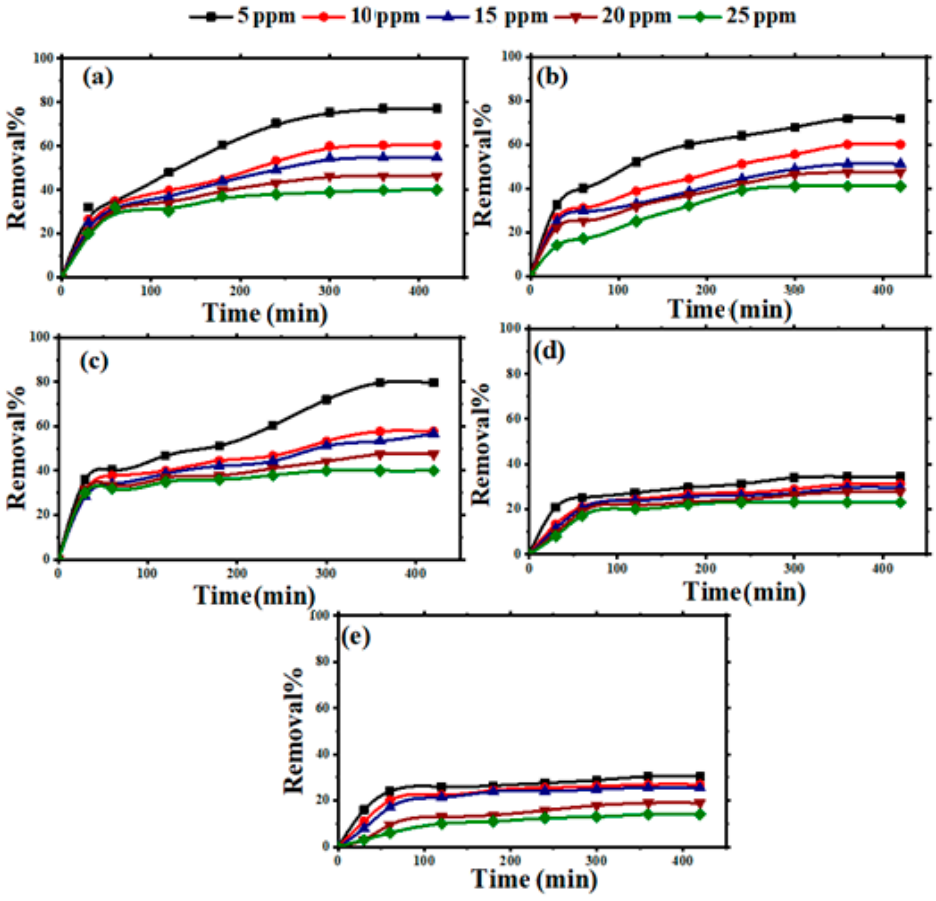


Figure 3. Effects of CR dye concentration and adsorption time on the removal% of CR dye at 25 °C and pH 7 with 20 mg of (**a**) GL (**b**) GLACT1M (**c**) GLACT2M (**d**) GLACT3M, and (**e**) GLACT4M.

Adsorption efficiency rises with lowering CR dye concentration, especially at 5 ppm. In comparison to pure and 1, 3, and 4 M NaOH-activated glauconite, activated glauconite with 2 M NaOH showed the highest elimination percentage (79.6%). Figure S2 further demonstrates that GLACT3M and GLACT4M adsorb a small amount of dye on their surfaces, with removal percentages of 34.4% and 30.4%, respectively. The order of the adsorbents is thus GLACT2M > GL > GLACT1M > GLACT3M > GLACT4M. The predominant chemical components of the GL used in this work are SiO_2 and Al_2O_3. However, in alkali treatment, the dissolution of Si prevailed over Al, and this might be the reason for the lower adsorption performance of GLACT3M and GLACT4M [51,52]. Also, it may be due to the destruction of iron sites in the GL surface that reduces the CR removal capability of glauconite [38]. As seen in Figure S2, the amount of adsorbed CR rises with rising CR concentration. This might be due to the concentration gradient being wider as the starting dye concentration rises. As a result, the driving force rises, making it suited for breaking down mass transfer resistance between CR adsorbate and adsorbent [52]. The maximum GL adsorption capacity was measured at pH 7 and 25 °C to be 3.9, 6.8, 9.3, and 11.0 mg/g at initial dye concentrations of 5, 10, 15, 20, and 25 mg/L, respectively. GLACT1M adsorption capacities are estimated to be 3.6, 5.9, 7.6, 9, and 10.3 mg/g, correspondingly, whereas GLACT2M adsorption capacities were 4.0, 5.7, 8.5, 9.5, and 10 mg/g. While the GLACT3M adsorption capacity was 1.72, 3.1, 4.4, 5.5, and 5.7 mg/g, the GLACT4M adsorption capacity was 1.52, 2.6, 3.8, 3.7, and 3.5 mg/g at pH 7 and 25 °C, respectively. The results show that modifying glauconite with 2 M NaOH is a viable technique for increasing the CR removal percentage using GL at lower concentrations. The existence of more active adsorption sites and a higher active surface area in nanoporous materials may be the cause of this improvement. NaOH activation aids in the removal of contaminants and increases the surface area of the layered glauconite [25]. The NaOH activation causes the glauconite layers to spread out, increasing the surface area. More active sites for the adsorption of CR molecules are provided by the increased surface area.

3.2.2. Effects of Adsorbent Doses

The influence of adsorbent dose on dye removal% was assessed to calculate the adsorption expenditure and to determine the optimal dose of the adsorbent that delivers the highest efficiency, as shown in Figure 4a. The adsorbent concentrations ranged from 0.02 to 0.1 g. For 20 mL of 5 mg/L CR solution, 0.02 g of adsorbent produces the highest efficiency, which was 79.6% for GLACT2M, 77.2% for GL, and 72% for GLACT1M, but only 34.4% and 30.4% for GLACT3M and GLACT4M, respectively.

This figure shows a reduction in the CR dye removal% when the adsorbent dose increased from 0.02 to 0.1 g for the five samples. For GLACT2M, the removal% declined to 67% when the dose was increased to 0.04 g and continued to fall to 32.4% as the dosage increased to 0.1 g. For GL adsorbent, the removal% fell to 63.6% when the dose was increased to 0.04 g, and it continued to fall to 29% with a 0.1 g dose. At a dose of 0.1 g, the removal percentage for GLACT1M decreased to 22.8%. The figure shows that GLACT3M and GLACT4M behaved similarly.

The decrease in the removal% with increasing adsorbent dose might be explained by the screening effect, which occurs as the adsorbent dosage increases and a thick layer is formed as a result of adsorbent particle accumulation and the reduction of the spaces among the adsorbent molecules. The thick, dense layers on the outermost surfaces of the adsorbents blocked further CR from attaching to the binding locations on the surface. Also, these agglomerations at high doses of adsorbents hinder the diffusion channels for CR adsorption, resulting in a reduction in adsorption percentage [25,53]. Moreover, the decrease in adsorption capability with increasing adsorbent density has been attributed to a variety of causes, including solutes accessibility, electrostatic interactions, interference between binding locations, and lesser mixing at higher adsorbent density [8,25]. The reported data agree with the data obtained by Sobeih et al. [35] and in contradiction with the data reported for the Malachite green's adsorption characteristics on natural red clay

by Sevim et al. [54], which show that increasing the adsorbent mass will cause an increase of adsorption rate due to increasing adsorption sites.

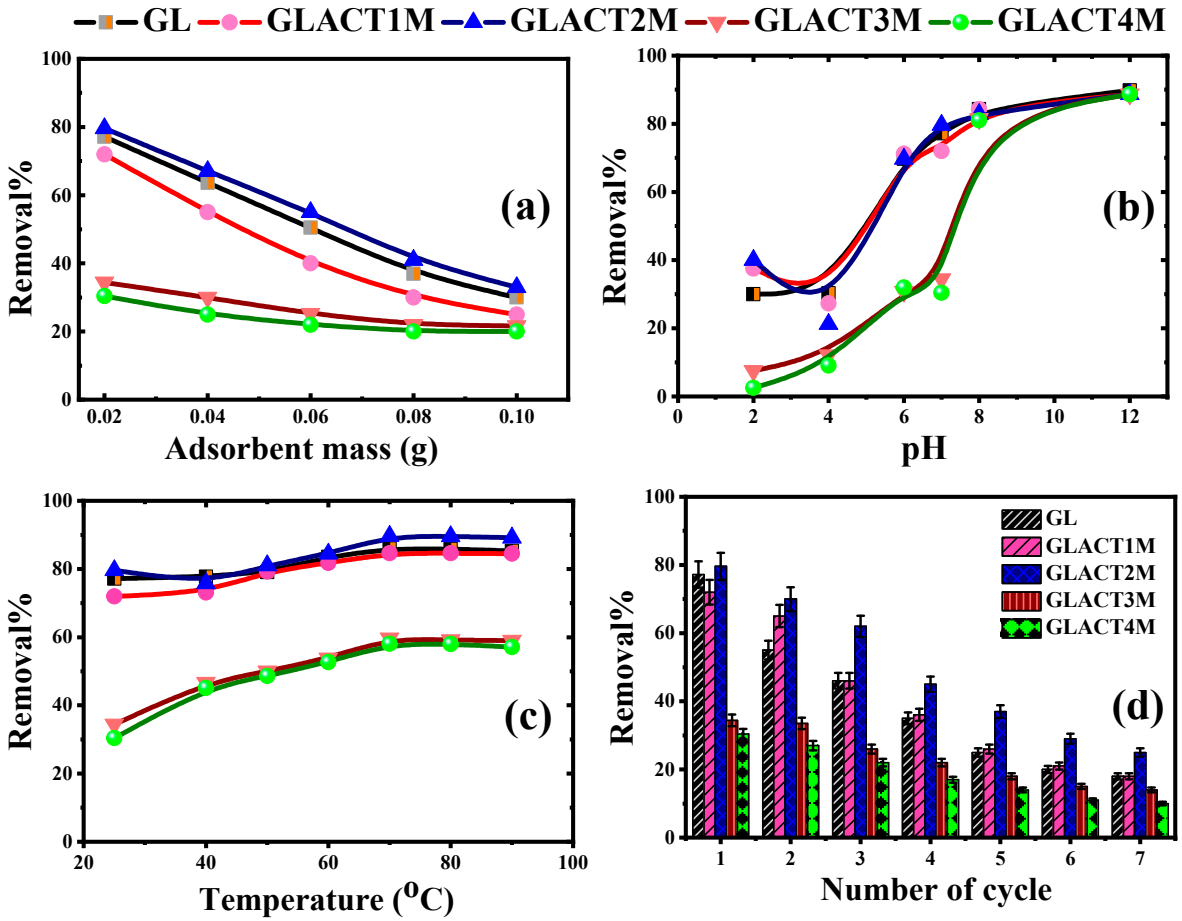


Figure 4. Effects of (**a**) adsorbent masses, (**b**) pH values, and (**c**) adsorption temperatures on the CR removal% (20 mL and 5 mg·L^{-1}) with GL, GLACT1M, GLACT2M, GLACT3M, and GLACT4M; and (**d**) the reusability test.

3.2.3. Effects of Solution pH

Because of the impact of pH changes on the ionization degrees of the adsorbent molecules and the adsorbent's surface characteristics, the influence of pH on the adsorption process has been studied [25]. Figure 4b illustrates the effect of pH on CR removal performance utilizing the produced adsorbents ranging from pH 2 to pH 12. The removal percentages employing 20 mg GL for 20 mL of 5 mg/L CR solution are 30.0, 30.3, 69.6, 77.2, 84.2, and 89.7% for pH 2, 4, 6, 7, 8, and 12, correspondingly. The GLACT1M adsorbent removes 37.5, 27, 71.2, 72, 84, and 88.6% under the same conditions, whereas the GLACT2M adsorbent removes 40, 21, 69.8, 79.6, 82.8, and 88.6%, respectively. Similar to this, as pH scaled from 2 to 12, the CR removal percentage rose from 7.5% to 88.6% and from 2.5% to 86.6% using GLACT3M and GLACT4M, respectively.

The influence of pH changes on the zeta potential of the adsorbent under investigation (GL) in an aqueous solution has been shown in Figure S3 (Supplementary Materials). The data revealed that the surface charge of GL is mostly negative within a pH ranging from 2 to 12. Moreover, with the gradual increase in pH, higher values of the surface charges are obtained, which in turn causes a noticeable more electrostatic interaction between the GL and CR negative molecules. Additionally, the observed changes in the zeta potential values indicate large fluctuations in adsorption capacity recorded for pH ranging from 4 to 7. Generally, the elimination percentage increases as the zeta potential value shifts more

positively. Since the adsorbent surface is somewhat negatively charged and the electrostatic reactions among GL and CR via the sulfonic acid groups (SO^{3-}) are primarily repulsive, the reduced zeta potential indicates that these forces are present [8], i.e., when the pH rises, fewer negatively charged locations are found on the adsorbent surfaces, while more positively charged locations are discovered. As a result, the anionic dye and positively charged surface interact electrostatically more strongly at higher pH levels, increasing adsorption. During the adsorption process at low pH values, H^+ ions compete with CR molecules, lowering the CR removal percentage [25].

3.2.4. Effects of Adsorption Temperatures

Adsorption temperature is a significant physicochemical processing factor because it results in an alteration in the adsorption capacities of the adsorbent [8,25]. The temperature impact on the removal% of CR onto GL, GLACT1M, GLACT2M, GLACT3M, and GLACT4M was investigated at various adsorption temperatures. Figure 4c shows the results of adsorption studies conducted at 25, 40, 50, 60, 70, 80, and 90 °C. When the temperatures rose from 25 to 70 °C, the CR removal percentage increased from 77.2% to 86%, 72% to 84%, and 79.6% to 89% for GL, GLACT1M, and GLACT2M, respectively. In the same sequence, it increased from 34.4% to 59% and from 30.4% to 58% for GLACT3M and GLACT4M. This performance may be explained by the increase in the CR diffusion rate as the temperature rose from 25 to 70 °C [55]. As the temperature increased from 70 to 90 °C, the percentage of dye removed remained constant. This tendency might be described by the fact that the CR molecules have occupied all active sites on the adsorbent surface. This behavior agreed well with the data presented by Khan et al. [56,57] and Arnata et al. [58].

3.2.5. Reusability of Adsorbents

The prior samples' reusability for CR removal was repeated four times without changing either the adsorbent or dose, Figure 4d. These results revealed that the removal percentage for all samples under investigation changed substantially through the four adsorption cycles. For the GL adsorbent, the CR removal percentages declined from 77.2% in the first cycle to 35% in the fourth cycle and eventually to 18% in the seventh cycle. The GLACT1M adsorbent's dye removal percentage falls from 72% in cycle one to 36% in cycle four and eventually to 18% in cycle seven. The CR removal percentage for GLACT2M adsorbent decreases from 79.6% to 45% from the first to fourth cycle and eventually to 25% in the seventh cycle. As the number of reuse cycles rises from one to seven, the percentages of dye adsorption for GLACT3M and GLACT4M adsorbents decrease from 34.4% to 14% and from 30.4% to 10%, respectively. The drop in CR adsorption percentage might be accredited to CR agglomerations on the surface of prior adsorbents, which reduces the adsorption capacity by shielding the adsorbent surface and pores from the dissolved CR molecules [8,25]. The results also indicate that the activation of GL with 2 M NaOH slightly improved the retained efficiency from 45.3% to 56.5% of its starting performance after four reusability cycles.

3.3. Adsorption Equilibrium Isotherms

To examine the adsorption isotherms, Langmuir, Freundlich, and Temkin isotherms are applied to fit the experimental data. The statistical significance of R^2 (correlation coefficient) for linear plots of C_e/q_e vs. C_e, $\log(q_e)$ vs. $\log(C_e)$, and q_e vs. $\mathrm{Ln}(C_e)$, Figure S4 (Supplementary Materials) was utilized. The calculated values from the linear plots for Q_o, K_L, K_F, $1/n$, K_T, B, and R^2 are shown in Table 2. In terms of correlation coefficients, the Freundlich and Langmuir models performed better than the Tempkin model, and the Freundlich model performed marginally better for the GL, GLACT1M, and GLACT3M data, proving that adsorption occurs on a heterogeneous surface. As a result, multilayer CR adsorption happens at active locations on the adsorbent surface, where there are unequally accessible heterogeneous sites, varying adsorption energies, and interactions between adsorbed molecules. The values of $1/n > 1$ imply that the CR adsorption is favorable at 25 °C,

which is advantageous for the chemisorption process [59]. This shows that the surfaces are varied as fewer interactions occur between adsorbed molecules [60]. The mechanism of CR adsorption onto GLACT2M and GLACT4M is slightly better fitted to the Langmuir model. Because the correlation coefficients for GLACT2M with Langmuir and Freundlich are 0.9687 and 0.9501 (<0.99), both models can be employed for describing the adsorption behavior of this adsorbent. This suggests that the adsorption process on the GLACT2M surface is likely to involve both multilayer adsorption and monolayer adsorption on a limited number of binding sites. The R_L values are between 0 and 1; therefore, GLACT2M is confirmed as a favorable adsorbent for Congo red dye [25]. Therefore, the modification procedure generated variations in surface-active locations from homogeneous to heterogeneous to provide non-monolayer coverage [39].

Table 2. Isotherms analysis for CR adsorption on GL, GLACT1M, GLACT2M, GLACT3M, and GLACT4M.

Langmuir Isotherm				
Adsorbent	Q_o **(mg/g)**	K_L **(L/mg)**	R_L	$\mathbf{R^2}$
GL	13.2	0.25	0.13	0.9725
GLACT1M	13.1	0.22	0.14	0.9850
GLACT2M	11.9	0.33	0.11	0.9687
GLACT3M	11.7	0.05	0.43	0.9430
GLACT4M	5.1	0.15	0.21	0.9302
Freundlich Isotherm				
Adsorbent	**1/*n***	K_f	$\mathbf{R^2}$	
GL	2.4172	3.59	0.9916	
GLACT1M	2.2048	3.13	0.9951	
GLACT2M	2.7400	3.87	0.9501	
GLACT3M	1.3716	0.75	0.9703	
GLACT4M	2.0240	0.93	0.8202	
Temkin Isotherm				
Adsorbent	**B (J/mol)**	K_T **(L/mole)**	$\mathbf{R^2}$	
GL	2.7463	3.0359	0.9552	
GLACT1M	2.8728	2.2784	0.9823	
GLACT2M	2.3737	4.4942	0.9257	
GLACT3M	2.4943	0.5774	0.9599	
GLACT4M	1.2315	1.2086	0.8078	

3.4. Adsorption Kinetics and Sorption Mechanisms

The CR adsorption process on GL, GLACT1M, GLACT2M, GLACT3M, and GLACT4M was examined at various values of the beginning dye concentration to establish the best kinetic model for adsorption. Figure 5 depicts the first-order, second-order, and Elovich kinetics plots of $\ln(q_e - q_t)$ vs. t, t/q_t vs. t, and q_t vs. $\ln(t)$. Table S2 (Supplementary Materials) displays the values of k_1, k_2, q_e, and R^2. The CR adsorption onto the indicated substances is well presented by the second order model, as seen by higher R^2 values ranging from 5 ppm to 25 ppm [61], except for ACT4M, which was a second order from 5 to 15 ppm and followed the Elovich model from 20 to 25 ppm. This shows that the rate-limiting phase for these adsorbents over the whole range of adsorption is chemical sorption or chemisorption, where the adsorption rate depends on adsorption capacity rather than adsorbate concentration. The data for ACT4M at high dye concentrations indicate that there is interaction between the adsorbed ions, the adsorption takes place at localized sites with a heterogeneous distribution of adsorption energies, and the adsorbate concentration is assumed to remain constant. Similar conclusions have been documented in the past by Younes et al. [39] and Indhu and Muthukumaran [48].

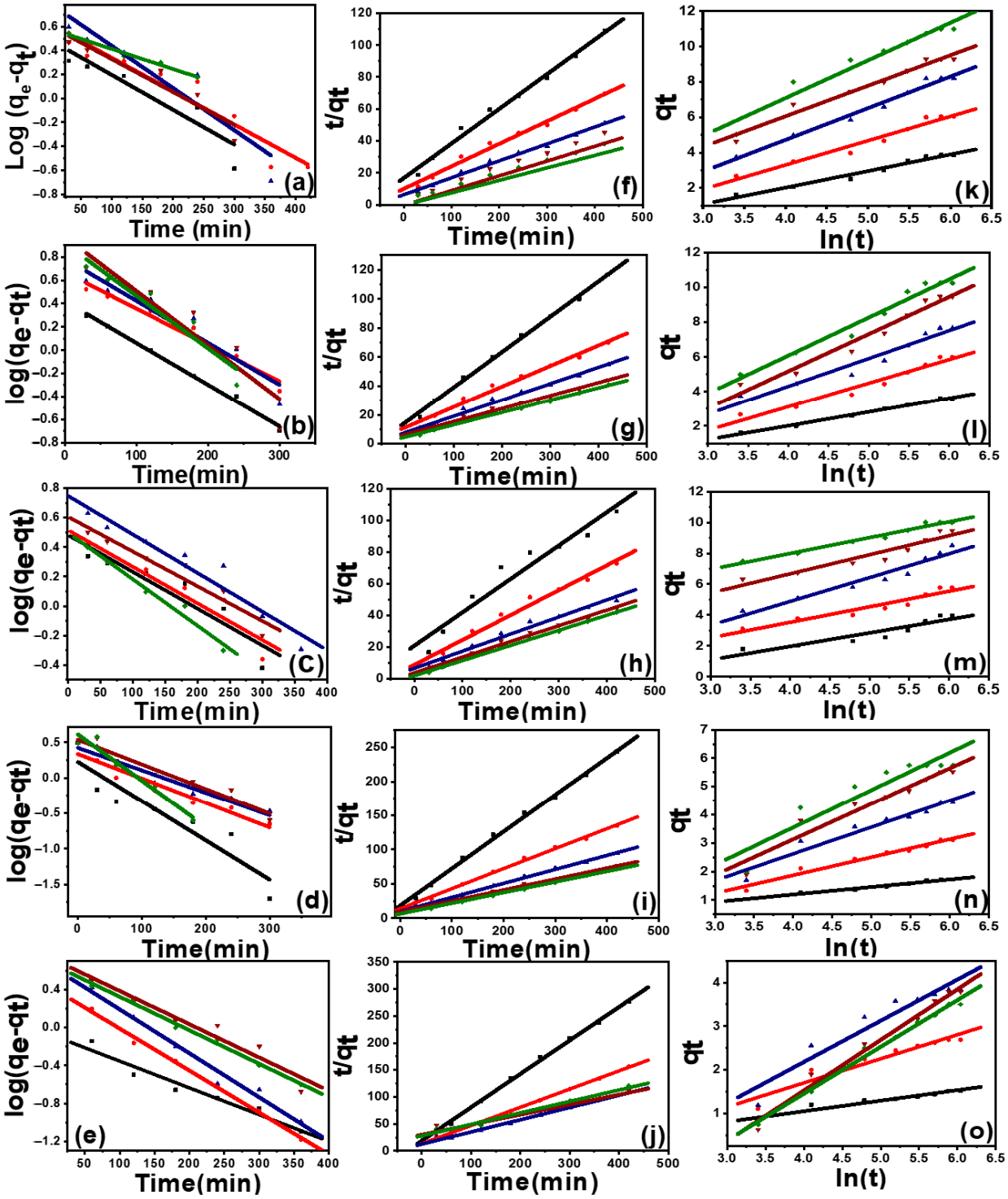


Figure 5. Plots of sorption kinetics for the adsorption of CR dye by 20 mg of GL (**a**,**f**,**k**), GLACT1M (**b**,**g**,**l**), GLACT2M (**c**,**h**,**m**), GLACT3M (**d**,**i**,**n**), and GLACT4M (**e**,**j**,**o**) at pH 7 and 25 °C; (**a**–**e**) pseudo-first-order, (**f**–**j**) pseudo-second-order, and (**k**–**o**) Elovich kinetic model.

To determine the mechanism as well as rate-controlling stages that affect adsorption kinetics, Weber's intra-particle model is applied to fit the practical data of 15 ppm CR solutions by 0.02 g of GL, GLACT2M, and GLACT4M [25]. A straight line in the q_t vs. $t^{1/2}$ graphic suggests the application of the intra-particle diffusion hypothesis. The results were multilinear with three linear phases (Figure 6), suggesting that two more phases, rather than only the intraparticle diffusion step, are accountable for controlling the adsorption reaction.

The first phase illustrates the impact of the boundary layer and external mass transfer, in which the CR was quickly absorbed by the used adsorbents. The second phase, which lasted for 300 min, began after the adsorption rate decreased after 60 min. This phase, according to Kumar and Porkodi [62,63], describes the diffusion of molecules to the adsorbent's most interior adsorption sites. After 300 min, the equilibrium phase was observed, which caused a drop in intraparticle diffusion since there were fewer available adsorption sites. Table S3 (Supplementary Materials) shows the results of calculating K_3 using the plot's slope in the three phases for GL, GLACT2M, and GLACT4M. The third phase's drop in k_3 value for GLACT2M indicates that the diffusion of CR molecules inside the adsorbent is the crucial stage in the adsorption process. Additionally, Figure 6's non-zero straight line intercept values suggest that other interaction mechanisms, such as surface adsorption and interior diffusion, may be active simultaneously with the intra-particle diffusion model due to the early rate-controlling mechanism in determining the kinetic of the adsorption reaction [64]. The intercept reflects the boundary layer impact. The contribution of the rate-control phase from surface adsorption increases with increasing intercept [25,64].

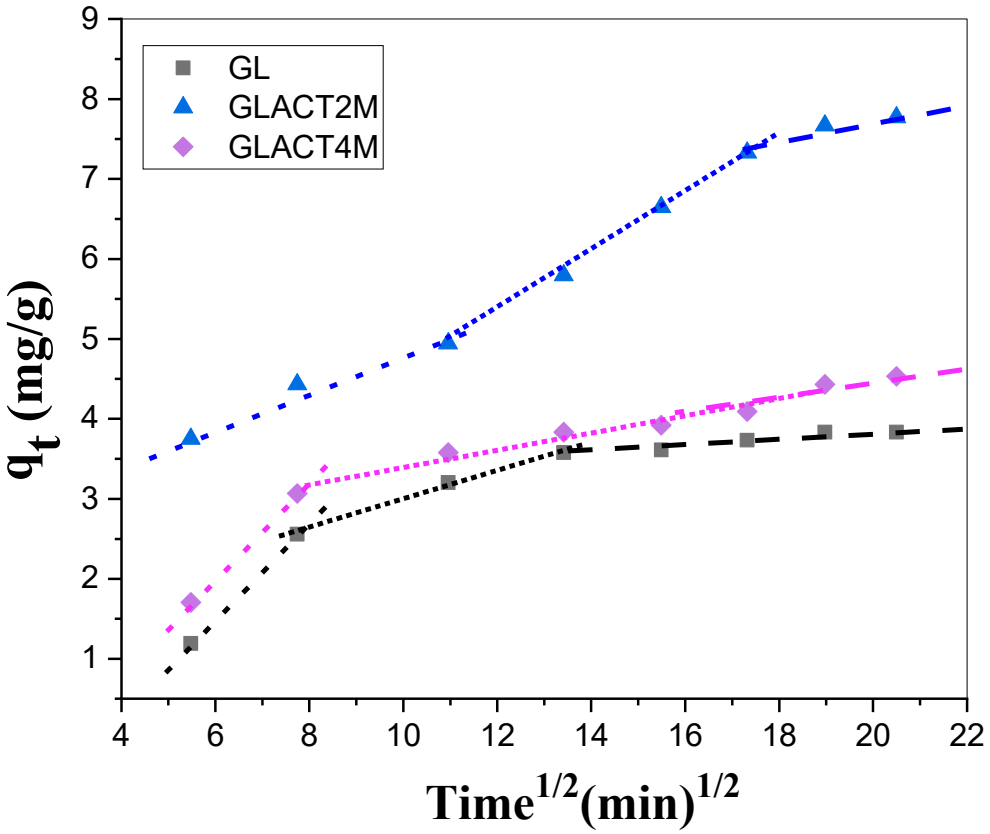


Figure 6. Intra-particle sorption kinetic of 15 ppm CR dye by 0.02 g of GL, GLACT2M, and GLACT4M.

In terms of CR dye adsorption capacity and CR removal% under different optimized conditions, Table 3's results compare our glauconite and NaOH-activated glauconite nanoadsorbents to other comparable adsorbents that have been reported previously [10,25,39,65–67]. The findings demonstrate that, even at very low doses, our new and improved GLACT2M nanoadsorbent outperforms most of the previously reported adsorbents in terms of dye removal% under the selected optimum conditions. Modified glauconite is an innovative, calming adsorbent for removing CR dye from wastewater. The maximum CR dye removal efficiency of 79.6% for NaOH-activated glauconite is a significant level of adsorption.

Table 3. Comparison between the CR dye adsorption capacity (Q_m) and CR removal% under the optimized conditions using our glauconite and NaOH-activated glauconite nanoadsorbents and other comparable benchmarks and GL-based adsorbents that have been reported previously.

Adsorbent	Conditions							Reference
	Dye	C_o (mg/L)	Dose (g/L)	pH	Time (min)	Q_m (mg/g)	R%	
Chemically modified rice husk char	CR	80	0.5	7	10–50	2.04	90%	[65]
Fly ash modified with 1 M, 3 M, 4 M HCl	CR	25–100	0.2	7	60	0.004, 0.74, 0.06		[66]
Phosphate-modified kaolinite	CR	25–300	0.1	3–8	5–600	-	65%	[10]
Thermally activated GL	RY160	10–80	1	1	180	-	64%	[39]
Acetic acid-activated GL	RY160	10–80	1	1	180	-	81%	[39]
GL/Polyaniline composite	CR	5–25	0.02	7	420	14.1	86%	[25]
Pinus pinaster bark	CR	5	10	2	10,080 (7 days)	1.6	100	[67]
GL GLACT1M GLACT2M GLACT3M GLACT4M	CR	5–25	0.02	7	360	13.2 13.1 11.9 11.7 5.1	79.6%	Present study

4. Conclusions

Using NaOH solutions at varying concentrations, natural glauconite was effectively activated and used in this investigation as an effective and inexpensive adsorbent for the CR dye from the textile effluent. The effects of starting dye concentration, reaction time, adsorbent dose, pH, temperature, and reusability on the dye removal percentage were examined. The outcomes showed that the 2 M NaOH/glauconite (GLACT2M) nanoadsorbent was capable of achieving the highest value (80%) of the CR removal percentage. The isotherm analysis results indicated that the experimental data fitted the Freundlich isotherm very well. While the Elovich model expresses the data of GLACT4 from 20 to 25 ppm, the pseudo-second-order model (R^2 = 0.998) properly explains the experimental data for GL, GLACT1M, GLACT2M, and GLACT3M from 5 to 25 ppm. According to the findings, CR dye was efficiently removed from textile effluent using natural, inexpensive adsorbents like NaOH-activated glauconite. Even though the results of this study are superior to the majority of glauconite-based adsorbents that have already been published, the claimed reusability is still constrained, and the efficiency has to be raised. For our upcoming investigation, we will use plasmonic support nanoparticles or/and a doping technique to generate a more efficient, stable, and reusable glauconite-based adsorbent in order to increase the expected nanoadsorbents' commercial feasibility.

Supplementary Materials: The following supporting information can be downloaded at https://www.mdpi.com/article/10.3390/w15213753/s1, Figure S1. Schematic representation for mechanism of interaction between CR and glauconite. Figure S2. Effect of CR dye concentrations and contact time on the adsorbed quantity of CR dye at 25 °C and pH 7 by 20 mg of (a) GL (b) GLACT1M (c) GLACT2M (d) GLACT3M and (e) GLACT4M. Figure S3. The zeta potential for Gl as a function of pH. Figure S4. Plots of adsorption isotherms for the adsorption of CR dye by 20 mg of GL, GLACT1M, GLACT2M, GLACT3M, and GLACT4M at 25 °C and pH 7. Table S1. Conditions of experimental tests. CR dye adsorption tests were carried out using a range of parameters, including starting dye

concentrations, adsorbent dosages, pH values, and temperatures. Table S2. Parameters of the kinetic models for CR dye adsorption on GL, GLACT1M, GLACT2M, GLACT3M, and GLACT4M. Table S3. Intra-particle diffusion constant for GL, GLACT2M, and GLACT4M for adsorption of 15 ppm CR at 25 °C.

Author Contributions: Conceptualization, D.S., A.H., N.K.S., A.M.E., S.I.A.-S., A.A.-G., R.E.-S., S.A.A. and M.S.; methodology, D.S., A.H., N.K.S., S.I.A.-S. and M.S.; validation, A.H., N.K.S., A.A.-G. and M.S.; formal analysis, D.S., A.H., N.K.S., A.A.-G., S.I.A.-S. and M.S.; investigation, D.S., A.H., N.K.S., A.M.E., A.A.M.E.-R., S.I.A.-S., A.A.-G., R.E.-S., S.A.A. and M.S.; resources, D.S., A.H., S.I.A.-S., R.E.-S. and M.S.; data curation, D.S., A.H., N.K.S., A.A.M.E.-R. and M.S.; writing—original draft preparation, D.S., A.H., N.K.S., H.F.A., S.I.A.-S. and M.S.; writing—review and editing, D.S., A.H., N.K.S., A.M.E., S.I.A.-S., A.A.-G., R.E.-S., S.A.A. and M.S.; visualization, D.S., A.H., N.K.S., A.A.M.E.-R. and M.S.; supervision, D.S., A.H., A.M.E., S.A.A. and M.S.; project administration, S.I.A.-S., A.A.-G. and M.S.; funding acquisition, S.I.A.-S., A.A.-G. and M.S. All authors have read and agreed to the published version of the manuscript.

Funding: Princess Nourah bint Abdulrahman University Researchers Supporting Project number (PNURSP2023R58), Princess Nourah bint Abdulrahman University, Riyadh, Saudi Arabia.

Data Availability Statement: The data presented in this study are available upon request from the corresponding author.

Acknowledgments: The authors express their gratitude to Princess Nourah bint Abdulrahman University Researchers Supporting Project number (PNURSP2023R58), Princess Nourah bint Abdulrahman University, Riyadh, Saudi Arabia.

Conflicts of Interest: The authors declare no conflict of interest.

References

1. Ruiz-Santoyo, V.; Andrade-Espinoza, B.A.; Romero-Toledo, R.; Anaya-Esparza, L.M.; Villagrán, Z.; Guerra-Contreras, A. Use of Nanostructured Photocatalysts for Dye Degradation: A Review. *Period. Polytech. Chem. Eng.* **2022**, *66*, 367–393. [CrossRef]
2. Joseph, C.G.; Taufiq-Yap, Y.H.; Affandi, N.A.; Nga, J.L.H.; Vijayan, V. Photocatalytic treatment of detergent-contaminated wastewater: A short review on current progress. *Korean J. Chem. Eng.* **2022**, *39*, 484–498. [CrossRef]
3. Rathoure, A.K.; Dhatwalia, V.K. *Toxicity and Waste Management Using Bioremediation*; Engineering Science Reference; IGI Global: Hershey, PA, USA, 2016.
4. Mukhopadhyay, R.; Bhaduri, D.; Sarkar, B.; Rusmin, R.; Hou, D.; Khanam, R.; Sarkar, S.; Biswas, J.K.; Vithanage, M.; Bhatnagar, A. Clay–polymer nanocomposites: Progress and challenges for use in sustainable water treatment. *J. Hazard. Mater.* **2020**, *383*, 121125. [CrossRef] [PubMed]
5. Mustapha, S.; Ndamitso, M.; Abdulkareem, A.; Tijani, J.; Shuaib, D.; Ajala, A.; Mohammed, A. Application of TiO_2 and ZnO nanoparticles immobilized on clay in wastewater treatment: A review. *Appl. Water Sci.* **2020**, *10*, 49. [CrossRef]
6. Varjani, S.; Rakholiya, P.; Shindhal, T.; Shah, A.V.; Ngo, H.H. Trends in dye industry effluent treatment and recovery of value added products. *J. Water Process Eng.* **2021**, *39*, 101734. [CrossRef]
7. Yaseen, D.A.; Scholz, M. Textile dye wastewater characteristics and constituents of synthetic effluents: A critical review. *Int. J. Environ. Sci. Technol.* **2019**, *16*, 1193–1226. [CrossRef]
8. Hamd, A.; Shaban, M.; Al Mohamadi, H.; Dryaz, A.R.; Ahmed, S.A.; Al-Ola, K.A.A.; El-Mageed, H.R.A.; Soliman, N.K. Novel Wastewater Treatment by Using Newly Prepared Green Seaweed–Zeolite Nanocomposite. *ACS Omega* **2022**, *7*, 11044–11056. [CrossRef]
9. Crini, G.; Lichtfouse, E. Advantages and disadvantages of techniques used for wastewater treatment. *Environ. Chem. Lett.* **2019**, *17*, 145–155. [CrossRef]
10. Mohamed, F.; Abukhadra, M.R.; Shaban, M. Removal of safranin dye from water using polypyrrole nanofiber/Zn-Felayered double hydroxide nanocomposite (Ppy NF/Zn-Fe LDH) of enhanced adsorption and photocatalytic properties. *Sci. Total Environ.* **2018**, *640*, 352–363. [CrossRef]
11. Ghabaee, S.; Behin, J.; Ansari, M.; Rajabi, L. Synthesis and characterization maleate-alumoxane nanoparticles for removal of reactive yellow 84 dye from aqueous solution. *Adv. Powder Technol.* **2020**, *31*, 2061–2071. [CrossRef]
12. Behin, J.; Farhadian, N. Response surface methodology and artificial neural network modeling of reactive red 33 decolorization by O_3/UV in a bubble column reactor. *Adv. Environ. Technol.* **2016**, *1*, 33–44.
13. Dutta, S.; Gupta, B.; Srivastava, S.K.; Gupta, A.K. Recent advances on the removal of dyes from wastewater using various adsorbents: A critical review. *Mater. Adv.* **2021**, *2*, 4497–4531. [CrossRef]
14. Feng, Y.; Zhou, H.; Liu, G.; Qiao, J.; Wang, J.; Lu, H.; Yang, L.; Wu, Y. Methylene blue adsorption onto swede rape straw (*Brassica napus* L.) modified by tartaric acid: Equilibrium, kinetic and adsorption mechanisms. *Bioresour. Technol.* **2012**, *125*, 138–144. [CrossRef] [PubMed]

15. Xue, H.; Gao, X.; Seliem, M.K.; Mobarak, M.; Dong, R.; Wang, X.; Fu, K.; Li, Q.; Li, Z. Efficient adsorption of anionic azo dyes on porous heterostructured MXene/biomass activated carbon composites: Experiments, characterization, and theoretical analysis via advanced statistical physics models. *Chem. Eng. J.* **2023**, *451*, 138735. [CrossRef]
16. Imessaoudene, A.; Cheikh, S.; Hadadi, A.; Hamri, N.; Bollinger, J.-C.; Amrane, A.; Tahraoui, H.; Manseri, A.; Mouni, L. Adsorption Performance of Zeolite for the Removal of Congo Red Dye: Factorial Design Experiments, Kinetic, and Equilibrium Studies. *Separations* **2023**, *10*, 57. [CrossRef]
17. Extross, A.; Waknis, A.; Tagad, C.V.V.; Gedam, P.D. Pathak. Adsorption of congo red using carbon from leaves and stem of water hyacinth: Equilibrium, kinetics, thermodynamic studies. *Int. J. Environ. Sci. Technol.* **2023**, *20*, 1607–1644. [CrossRef]
18. Rose, P.K.; Poonia, V.; Kumar, R.; Kataria, N.; Sharma, P.; Lamba, J.; Bhattacharya, P. Congo red dye removal using modified banana leaves: Adsorption equilibrium, kinetics, and reusability analysis. *Groundw. Sustain. Dev.* **2023**, *23*, 101005. [CrossRef]
19. Rubangakene, N.O.; Elwardany, A.; Fujii, M.; Sekiguchi, H.; Elkady, M.; Shokry, H. Biosorption of Congo Red dye from aqueous solutions using pristine biochar and ZnO biochar from green pea peels. *Chem. Eng. Res. Des.* **2023**, *189*, 636–651. [CrossRef]
20. Mortada, W.I.; Nabieh, K.A.; Abdelghany, A.M. Efficient and Low-Cost Surfactant-Assisted Solid Phase Extraction Procedure For Removal Of Methylene Blue Using Natural Dolomite. *Water Air Soil Pollut.* **2023**, *234*, 363. [CrossRef]
21. Ali, I.; Asim, M.; Khan, T.A. Low cost adsorbents for the removal of organic pollutants from wastewater. *J. Environ. Manag.* **2012**, *113*, 170–183. [CrossRef]
22. Wang, W.; Wang, A. Perspectives on green fabrication and sustainable utilization of adsorption materials for wastewater treatment. *Chem. Eng. Res. Des.* **2022**, *187*, 541–548. [CrossRef]
23. Fan, Q.; Wang, L.; Fu, Y.; Li, Q.; Liu, Y.; Wang, Z.; Zhu, H. Iron redox cycling in layered clay minerals and its impact on contaminant dynamics: A review. *Sci. Total Environ.* **2023**, *855*, 159003. [CrossRef] [PubMed]
24. Yang, G. Sorption and reduction of hexavalent uranium by natural and modified silicate minerals: A review. *Environ. Chem. Lett.* **2023**, *21*, 2441–2470. [CrossRef]
25. Salah, D.; Hamd, A.; Soliman, N.K.; Elzanaty, A.M.; Alanazi, A.M.; Shaban, M.; El-Sayed, R.; Ahmed, S.A. Polyaniline/Glauconite Nanocomposite Adsorbent for Congo Red Dye from Textile Wastewater. *Separations* **2022**, *9*, 384. [CrossRef]
26. Mohan, C.; Kumari, N.; Jindal, R.; Gautam, R. Application of Efficient Naturally Occurring Clay Mineral for Fuchsin Basic Dye Removal. In *Advances in Functional and Smart Materials*; Prakash, C., Singh, S., Krolczyk, G., Eds.; Lecture Notes in Mechanical Engineering; Springer: Singapore, 2023. [CrossRef]
27. Mohamed, F.; Hassaballa, S.; Shaban, M.; Ahmed, A.M. Highly Efficient Photocatalyst Fabricated from the Chemical Recycling of Iron Waste and Natural Zeolite for Super Dye Degradation. *Nanomaterials* **2022**, *12*, 235. [CrossRef] [PubMed]
28. Altowyan, A.S.; Shaban, M.; Faidey, Z.M.; Abdelkarem, K.; Al-Dossari, M.; Abd El-Gawaad, N.S.; Kordy, M.G.M. Design and Characterization of Zeolite/Serpentine Nanocomposite Photocatalyst for Solar Hydrogen Generation. *Materials* **2022**, *15*, 6325. [CrossRef]
29. Jennifer, E.C.; Ifedi, O.P. Modification of natural bentonite clay using cetyl trimethyl-ammonium bromide and its adsorption capability on some petrochemical wastes. *Chem. Int.* **2019**, *5*, 269–273.
30. Awwad, A.; Amer, M.; Al-aqarbeh, M.M. TiO_2-kaolinite nanocomposite prepared from the Jordanian Kaolin clay: Adsorption and thermodynamics of Pb (II) and Cd (II) ions in aqueous solution. *Chem. Int.* **2020**, *6*, 168–178.
31. Kausar, A.; Sher, F.; Hazafa, A.; Javed, A.; Sillanpää, M.; Iqbal, M. Biocomposite of sodium-alginate with acidified clay for wastewater treatment: Kinetic, equilibrium and thermodynamic studies. *Int. J. Biol. Macromol.* **2020**, *161*, 1272–1285. [CrossRef]
32. Alasadi, A.; Khaili, F.; Awwad, A.M. Adsorption of Cu (II), Ni (II) and Zn (II) ions by nano kaolinite: Thermodynamics and kinetics studies. *Chem. Int.* **2019**, *5*, 226–258.
33. Zehhaf, A.; Benyoucef, A.; Quijada, C.; Taleb, S.; Morallon, E. Algerian natural montmorillonites for arsenic (III) removal in aqueous solution. *Int. J. Environ. Sci. Technol.* **2015**, *12*, 595–602. [CrossRef]
34. Selby, D. U-Pb zircon geochronology of the Aptian/Albian boundary implies that the GL-O international glauconite standard is anomalously young. *Cretac. Res.* **2009**, *30*, 1263–1267. [CrossRef]
35. Sobeih, M.M.; El-Shahat, M.F.; Osman, A.; Zaid, M.A.; Nassar, M.Y. Glauconite clay-functionalized chitosan nanocomposites for efficient adsorptive removal of fluoride ions from polluted aqueous solutions. *RSC Adv.* **2020**, *10*, 25567–25585. [CrossRef] [PubMed]
36. Ali, O.; Osman, H.H.; Sayed, S.A.; Shalabi, M.E.H. The removal of uranium and thorium from their aqueous solutions via glauconite. *Desalination Water Treat.* **2015**, *53*, 760–767. [CrossRef]
37. Petrushka, I.M.; Gumnitskii, Y.M.; Malovanyi, M.S. External diffusion kinetics of the adsorption of anionic red 8C dye on glauconite. *Theor. Found Chem. Eng.* **2013**, *47*, 144–148. [CrossRef]
38. Oliver, J.; Hao, C.M.; Huang, T.C.P. The removal of metals and ammonium by natural glauconite. *Environ. Int.* **1987**, *13*, 203–212.
39. Younes, H.; El-Etriby, H.K.; Mahanna, H. High removal efficiency of reactive yellow 160 dye from textile wastewater using natural and modified glauconite. *Int. J. Environ. Sci. Technol.* **2022**, *19*, 5659–5674. [CrossRef]
40. Novikova, L.A.; Bel'chinskaya, L.I.; Krupskaya, V.V.; Roessner, F.; Zhabin, A.V. In Effect of acid and alkaline treatment on physicalchemical properties of surface of natural glauconite. *Sorpt. Chromatogr. Process.* **2015**, *15*, 730–740.
41. Wang, J.; Guo, X. Adsorption isotherm models: Classification, physical meaning, application and solving method. *Chemosphere* **2020**, *258*, 127279. [CrossRef]

42. Singh, S.A.; Vemparala, B.; Madras, G. Adsorption kinetics of dyes and their mixtures with Co_3O_4–ZrO_2 composites. *J. Environ. Chem. Eng.* **2015**, *3*, 2684–2696. [CrossRef]
43. Gan, C.; Liu, Y.; Tan, X.; Wang, S.; Zeng, G.; Zheng, B.; Li, T.; Jiang, Z.; Liu, W. Effect of porous zinc–biochar nanocomposites on Cr (VI) adsorption from aqueous solution. *RSC Adv.* **2015**, *5*, 35107–35115. [CrossRef]
44. Nassar, M.Y.; Ahmed, I.S.; Raya, M.A. A facile and tunable approach for synthesis of pure silica nanostructures from rice husk for the removal of ciprofloxacin drug from polluted aqueous solutions. *J. Mol. Liq.* **2019**, *282*, 251–263. [CrossRef]
45. Shekhar, S.; Mishra, D.; Agrawal, A.; Sahu, K.K. Physical and chemical characterization and recovery of potash fertilizer from glauconitic clay for agricultural application. *Appl. Clay Sci.* **2017**, *143*, 50–56. [CrossRef]
46. Huang, J.; Liu, Y.; Jin, Q.; Wang, X.; Yang, J. Adsorption studies of a water soluble dye, Reactive Red MF-3B, using sonication-surfactant-modified attapulgite clay. *J. Hazard. Mater.* **2007**, *143*, 541–548. [CrossRef]
47. Selim, K.; Youssef, M.; El-Rahiem, F.A.; Hassan, M. Dye removal using some surface modified silicate minerals. *Int. J. Min. Sci. Technol.* **2014**, *24*, 183–189. [CrossRef]
48. Indhu, S.; Muthukumaran, K. Removal and recovery of reactive yellow 84 dye from wastewater and regeneration of functionalised Borassus flabellifer activated carbon. *J. Environ. Chem. Eng.* **2018**, *6*, 3111–3121.
49. Younes, H.; Mahanna, H.; El-Etriby, H.K. Fast adsorption of phosphate (PO^{4-}) from wastewater using glauconite. *Water Sci. Technol.* **2019**, *80*, 1643–1653. [CrossRef]
50. Ibrahim, S.S.; El Kammar, A.M.; Guda, A.M.; Boulos, T.R.; Saleh, A. Characterization and mineral beneficiation of Egyptian glauconite for possible industrial use. *Part. Sci. Technol.* **2019**, *37*, 141–150. [CrossRef]
51. Oghenejohoh, K.; Ohimor, E. Effect of sodium hydroxide concentration on the physical properties of zeolite produced from local clay found in Nigeria's Niger Delta. *Eur. J. Sci. Res.* **2011**, *56*, 445–452.
52. Sharma, Y.C. Optimization of parameters for adsorption of methylene blue on a low-cost activated carbon. *J. Chem. Eng. Data* **2010**, *55*, 435–439. [CrossRef]
53. Mohamed, H.S.; Soliman, N.; Abdelrheem, D.A.; Ramadan, A.A.; Elghandour, A.H.; Ahmed, S.A. Adsorption of Cd^{2+} and Cr^{3+} ions from aqueous solutions by using residue of Padina gymnospora waste as promising low-cost adsorbent. *Heliyon* **2019**, *5*, e01287. [CrossRef] [PubMed]
54. Sevim, F.; Lacin, O.; Ediz, E.F.; Demir, F. Adsorption capacity, isotherm, kinetic, and thermodynamic studies on adsorption behavior of malachite green onto natural red clay. *Environ. Prog. Sustain. Energy* **2021**, *40*, e13471. [CrossRef]
55. Alkan, M.; Demirbaş, Ö.; Çelikçapa, S.; Doğan, M. Sorption of acid red 57 from aqueous solution onto sepiolite. *J. Hazard. Mater.* **2004**, *116*, 135–145. [CrossRef]
56. Khan, M.I.; Zafar, S.; Buzdar, A.R.; Azhar, M.F.; Hassan, W.; Aziz, A. Use of citrus sinensis leaves as a bioadsorbent for removal of congo red dye from aqueous solution. *Fresenius Environ. Bull.* **2018**, *27*, 4679–4688.
57. Khan, M.I.; Zafar, S.; Khan, M.A.; Mumtaz, F.; Prapamonthon, P.; Buzdar, A.R. Bougainvillea glabra leaves for adsorption of congo red from wastewater. *Fresenius Environ. Bull.* **2018**, *27*, 1456–1465.
58. Arnata, I.W.; Suprihatin, S.; Fahma, F.; Richana, N.; Sunarti, T.C. Adsorption of anionic congo red dye by using cellulose from sago frond. *Poll Res.* **2019**, *38*, 43–53.
59. Hamzeh, Y.; Ashori, A.; Azadeh, E.; Abdulkhani, A. Removal of Acid Orange 7 and Remazol Black 5 reactive dyes from aqueous solutions using a novel biosorbent. *Mater. Sci. Eng. C.* **2012**, *32*, 1394–1400. [CrossRef]
60. Sellaoui, L.; Guedidi, H.; Knani, S.; Reinert, L.; Duclaux, L.; Ben Lamine, A. Application of statistical physics formalism to the modeling of adsorption isotherms of ibuprofen on activated carbon. *Fluid Phase Equilibria* **2015**, *387*, 103–110. [CrossRef]
61. Raval, N.P.; Kumar, M. Geogenic arsenic removal through core–shell based functionalized nanoparticles: Groundwater in-situ treatment perspective in the post–COVID anthropocene. *J. Hazard. Mater.* **2021**, *402*, 123466. [CrossRef]
62. Kumar, K.V.; Porkodi, K. Mass transfer, kinetics and equilibrium studies for the biosorption of methylene blue using Paspalum notatum. *J. Hazard. Mater.* **2007**, *146*, 214–226. [CrossRef]
63. Campos, N.F.; Barbosa, C.M.; Rodríguez-Díaz, J.M.; Duarte, M.M. Removal of naphthenic acids using activated charcoal: Kinetic and equilibrium studies. *Adsorpt. Sci. Technol.* **2018**, *36*, 1405–1421. [CrossRef]
64. Weber, W.J., Jr.; Morris, J.C. Kinetics of adsorption on carbon from solution. *J. Sanit. Eng. Div.* **1963**, *89*, 31–59. [CrossRef]
65. Malik, A.; Khan, A.; Anwar, N.; Naeem, M. A comparative study of the adsorption of congo red dye on rice husk, rice husk char and chemically modified rice husk char from aqueous media. *Bull. Chem. Soc. Ethiop.* **2020**, *34*, 41–54. [CrossRef]
66. Augustus, E.N.; Samuel, A.S.; Nimibofa, A.; Donbebe, W. Removal of congo red from aqueous solutions using fly ash modified with hydrochloric acid. *Br. J. Appl. Sci. Technol.* **2017**, *20*, 1–7. [CrossRef]
67. Litefti, K.; Freire, M.S.; Stitou, M.; González-Álvarez, J. Adsorption of an anionic dye (Congo red) from aqueous solutions by pine bark. *Sci. Rep.* **2019**, *9*, 16530. [CrossRef]

Disclaimer/Publisher's Note: The statements, opinions and data contained in all publications are solely those of the individual author(s) and contributor(s) and not of MDPI and/or the editor(s). MDPI and/or the editor(s) disclaim responsibility for any injury to people or property resulting from any ideas, methods, instructions or products referred to in the content.